Measurement and correction of *in vivo* sample aberrations employing a nonlinear guide-star in two-photon excited fluorescence microscopy

Rodrigo Aviles-Espinosa,[1] Jordi Andilla,[2] Rafael Porcar-Guezenec,[2] Omar E. Olarte,[1] Marta Nieto,[3] Xavier Levecq,[2] David Artigas,[1,4] and Pablo Loza-Alvarez[1,*]

[1]*ICFO-The Institute of Photonic Sciences, Mediterranean Technology Park, Av. Canal Olimpic s/n, 08860 Castelldefels (Barcelona), Spain*
[2]*Imagine Optic, 18 rue Charles de Gaulle, 91400 Orsay, France*
[3]*CNB-CSIC, Darwin 3 28049 Madrid, Spain*
[4]*Department of Signal Theory and Communications, Universitat Politècnica de Catalunya, 08034 Barcelona, Spain*
**pablo.loza@icfo.es*

Abstract: We demonstrate that sample induced aberrations can be measured in a nonlinear microscope. This uses the fact that two-photon excited fluorescence naturally produces a localized point source inside the sample: the nonlinear guide-star (NL-GS). The wavefront emitted from the NL-GS can then be recorded using a Shack-Hartmann sensor. Compensation of the recorded sample aberrations is performed by the deformable mirror in a single-step. This technique is applied to fixed and *in vivo* biological samples, showing, in some cases, more than one order of magnitude improvement in the total collected signal intensity.

OCIS codes: (170.3880) Medical and biological imaging; (180.4315) Nonlinear microscopy; (190.4180) Multiphoton processes; (220.1080) Active or adaptive optics; (220.1000) Aberration compensation

References and links

1. W. Denk, J. H. Strickler, and W. W. Webb, "Two-photon laser scanning fluorescence microscopy," Science **248**(4951), 73–76 (1990).
2. P. T. C. So, C. Y. Dong, B. R. Masters, and K. M. Berland, "Two-photon excitation fluorescence microscopy," Annu. Rev. Biomed. Eng. **2**(1), 399–429 (2000).
3. M. J. Booth and T. Wilson, "Refractive-index-mismatch induced aberrations in single-photon and two-photon microscopy and the use of aberration correction," J. Biomed. Opt. **6**(3), 266–272 (2001).
4. D. Ganic, X. S. Gan, and M. Gu, "Reduced effects of spherical aberration on penetration depth under two-photon excitation," Appl. Opt. **39**(22), 3945–3947 (2000).
5. F. Helmchen and W. Denk, "Deep tissue two-photon microscopy," Nat. Methods **2**(12), 932–940 (2005).
6. M. A. A. Neil, R. Juskaitis, M. J. Booth, T. Wilson, T. Tanaka, and S. Kawata, "Adaptive aberration correction in a two-photon microscope," J. Microsc. **200**(2), 105–108 (2000).
7. D. Débarre, E. J. Botcherby, T. Watanabe, S. Srinivas, M. J. Booth, and T. Wilson, "Image-based adaptive optics for two-photon microscopy," Opt. Lett. **34**(16), 2495–2497 (2009).
8. J. M. Bueno, E. J. Gualda, and P. Artal, "Adaptive optics multiphoton microscopy to study *ex vivo* ocular tissues," J. Biomed. Opt. **15**(6), 066004 (2010).
9. Z. Kam, P. Kner, D. Agard, and J. W. Sedat, "Modelling the application of adaptive optics to wide-field microscope live imaging," J. Microsc. **226**(1), 33–42 (2007).
10. M. J. Booth, M. Schwertner, and T. Wilson, "Specimen-induced aberrations and adaptive optics for microscopy," Proc. SPIE **5894**, 26–34 (2005).
11. J. W. Cha, J. Ballesta, and P. T. C. So, "Shack-Hartmann wavefront-sensor-based adaptive optics system for multiphoton microscopy," J. Biomed. Opt. **15**(4), 046022 (2010).
12. D. Debarre, M. J. Booth, and T. Wilson, "Image based adaptive optics through optimisation of low spatial frequencies," Opt. Express **15**(13), 8176–8190 (2007).
13. M. J. Booth, "Wave front sensor-less adaptive optics: a model-based approach using sphere packings," Opt. Express **14**(4), 1339–1352 (2006).
14. P. N. Marsh, D. Burns, and J. M. Girkin, "Practical implementation of adaptive optics in multiphoton microscopy," Opt. Express **11**(10), 1123–1130 (2003).

#154177 - $15.00 USD Received 7 Sep 2011; revised 17 Oct 2011; accepted 20 Oct 2011; published 25 Oct 2011

15. W. Lubeigt, S. P. Poland, G. J. Valentine, A. J. Wright, J. M. Girkin, and D. Burns, "Search-based active optic systems for aberration correction in time-independent applications," Appl. Opt. **49**(3), 307–314 (2010).
16. J. M. Girkin, J. Vijverberg, M. Orazio, S. Poland, and A. J. Wright, "Adaptive optics in confocal and two-photon microscopy of rat brain: a single correction per optical section," Proc. SPIE **6442**, 64420T, 64420T-7 (2007).
17. A. J. Wright, D. Burns, B. A. Patterson, S. P. Poland, G. J. Valentine, and J. M. Girkin, "Exploration of the optimisation algorithms used in the implementation of adaptive optics in confocal and multiphoton microscopy," Microsc. Res. Tech. **67**(1), 36–44 (2005).
18. P. Kner and Z. Kam, "Adaptive optics takes tissue imaging to the next level," BioOpt. World **1**, 32–34 (2008).
19. M. Rueckel, J. A. Mack-Bucher, and W. Denk, "Adaptive wavefront correction in two-photon microscopy using coherence-gated wavefront sensing," Proc. Natl. Acad. Sci. U.S.A. **103**(46), 17137–17142 (2006).
20. M. J. Booth, "Adaptive optics in microscopy," Philos. Transact. A Math. Phys. Eng. Sci. **365**(1861), 2829–2843 (2007).
21. F. Roddier, *Adaptive Optics in Astronomy* (Cambridge University Press, 1999), Chap. 2.
22. O. Azucena, J. Crest, J. A. Cao, W. Sullivan, P. Kner, D. Gavel, D. Dillon, S. Olivier, and J. Kubby, "Wavefront aberration measurements and corrections through thick tissue using fluorescent microsphere reference beacons," Opt. Express **18**(16), 17521–17532 (2010).
23. G. Cormack, P. Loza-Alvarez, L. Sarrado, S. Tomas, I. Amat-Roldan, L. Torner, D. Artigas, J. Guitart, J. Pera, and J. Ros, "Lost writing uncovered by laser two-photon fluorescence provides a *terminus post quem* for Roman colonization of Hispania Citerior," J. Archaeol. Sci. **34**(10), 1594–1600 (2007).
24. R. Aviles-Espinosa, G. Filippidis, C. Hamilton, G. Malcolm, K. J. Weingarten, T. Südmeyer, Y. Barbarin, U. Keller, S. I. C. O. Santos, D. Artigas, and P. Loza-Alvarez, "Compact ultrafast semiconductor disk laser: targeting GFP based nonlinear applications in living organisms," Biomed. Opt. Express **2**(4), 739–747 (2011).
25. R. Kerr, V. Lev-Ram, G. Baird, P. Vincent, R. Y. Tsien, and W. R. Schafer, "Optical imaging of calcium transients in neurons and pharyngeal muscle of *C. elegans*," Neuron **26**(3), 583–594 (2000).
26. H. Tabata and K. Nakajima, "Efficient *in utero* gene transfer system to the developing mouse brain using electroporation: visualization of neuronal migration in the developing cortex," Neuroscience **103**(4), 865–872 (2001).
27. O. Azucena, J. Crest, S. Kotadia, W. Sullivan, X. Tao, M. Reinig, D. Gavel, S. Olivier, and J. Kubby, "Adaptive optics wide-field microscopy using direct wavefront sensing," Opt. Lett. **36**(6), 825–827 (2011).
28. M. J. Booth, M. A. A. Neil, and T. Wilson, "Aberration correction for confocal imaging in refractive-index-mismatched media," J. Microsc. **192**(2), 90–98 (1998).
29. V. A. Hovhannisyan, P. J. Su, and C. Y. Dong, "Characterization of optical-aberration-induced lateral and axial image inhomogeneity in multiphoton microscopy," J. Biomed. Opt. **13**(4), 044023 (2008).
30. E. Theofanidou, L. Wilson, W. J. Hossack, and J. Arlt, "Spherical aberration correction for optical tweezers," Opt. Commun. **236**(1-3), 145–150 (2004).
31. C. Y. Dong, B. Yu, P. D. Kaplan, and P. T. C. So, "Performances of high numerical aperture water and oil immersion objective in deep-tissue, multi-photon microscopic imaging of excised human skin," Microsc. Res. Tech. **63**(1), 81–86 (2004).
32. X. Tao, B. Fernandez, O. Azucena, M. Fu, D. Garcia, Y. Zuo, D. C. Chen, and J. Kubby, "Adaptive optics confocal microscopy using direct wavefront sensing," Opt. Lett. **36**(7), 1062–1064 (2011).

1. Introduction

Nonlinear microscopy (NLM) has several inherent advantages in contrast with confocal laser scanning microscopy. These are intrinsic optical sectioning, larger penetration depths, reduced photo damage etc. This has allowed the technique to become an important tool in biology [1]. These advantages rely on the fact that NLM is based on a multi-photon effect where the generated signals are nonlinearly dependent on the excitation intensity. This can be achieved when photons of ultrashort pulses are tightly focused through a high Numerical Aperture (NA) microscope objective resulting in a confined focal excitation volume [1,2]. Although this technique allows larger penetration depths compared with confocal microscopy, aberration effects and scattering limit the full exploitation of such capability. Aberrations lead to a spreading of the focusing spot inside the sample, both in axial and lateral directions, reducing the resolution and the intensity. As a consequence, the contrast of the imaged sample drops drastically [3–5]. Aberrations in a microscope are not only caused by the intrinsic optical elements quality and alignment, but also by the refractive index mismatch from the objective, immersion media, cover glass, and more importantly, by the inhomogeneous structure of biological samples [6]. In addition, when imaging inside semi-transparent samples, the image quality is weakly affected by scattering up to a depth of several scattering lengths [7].

To deal with these problems, microscopists are starting to adopt different Adaptive Optics (AO) sensing schemes to correct the aberrated wavefronts (WF). Such WF can be corrected in

#154177 - $15.00 USD Received 7 Sep 2011; revised 17 Oct 2011; accepted 20 Oct 2011; published 25 Oct 2011

the excitation beam [8], in the collected signal beam or in both. For example, in wide field techniques such as PALM or STORM, only the correction of the collected signal is important in order to maintain the contrast of the acquired images [9]. In confocal microscopy, both the excitation and collected beams need to be compensated to improve the intensity of the reconstructed images [10,11]. In NLM, there is no need to correct on the collected beam as no confocal aperture is required. However, correcting the excitation beam is a must as this will ensure a better focusing and therefore, a more efficient nonlinear (NL) process.

In practice, measuring and correcting excitation beam aberrations at the sample plane of a nonlinear microscope is a difficult task. Nevertheless, some strategies to do this have already been implemented. These strategies can be divided into sensor-based and sensor-less techniques.

In sensor-less schemes, iterative algorithms are generally used to control a deformable mirror (DM) or a Spatial Light Modulator [12,13]. This compensates the unknown existing optical aberrations without having to measure them. Although effective, optimization is performed by improving a merit function based on an image-quality related parameter, such as the total intensity within the imaged area [14,15]. The success of the algorithm is dependent on the initial guess of the optimization process, the employed algorithm, (genetic, modal, etc.) and the stopping criteria. Although it has been reported the use of optimized algorithms that reduce sample exposure [7,16], this still implies that an area of interest within the sample has to be exposed a considerable number of times. This may result in unwanted exposure which is prone to produce photo-bleaching and photo-toxic effects on the sample [17].

In sensor-based schemes, the correction can be performed by measuring the optical aberrations through a sensing device such as a wavefront sensor (WFS) or an interferometer [6,18,19]; then the information is then fed into an adaptive element. The standard implementation of this technique, when used for microscopy applications, suffers from important drawbacks. Collecting the excitation beam in forward direction requires careful consideration: first, because the upper layers of the sample will produce aberrations that might interfere with the measurement if the lower layers are being corrected, and second because an additional lens with the same or higher numerical aperture than the used microscope objective must be introduced into the setup. In this case, the optical quality and alignment of this element with the optical axis induces undesirable aberrations that must be calibrated. In a backward configuration the backscattered excitation signal (normally collected in double pass scheme) has the same intensity level as the spurious reflections, making it difficult to distinguish between these two [11,19,20].

Despite that, sensor based schemes are powerful techniques as WF aberrations are directly obtained. Thus, alternative solutions can be considered. Interferometric methods or confocal depth selection mechanisms have been successfully applied for a direct WF measurement. These principles have proved to work well as they enable to filter/select the excitation beam at the imaged focal plane. However, they work only in thick and highly scattering samples [11] or rely on complex experimental setups [19].

Given this, other methodologies, similar to those already used in astronomy, have been used. In particular AO has been broadly used in astronomy to compensate for the changing turbulent medium in the atmosphere which produces aberrations and deteriorates the image of objects to be observed. By employing a WFS it is possible to measure the distortions produced when distant light sources travel through the changing atmosphere, employing a reference point source called guide star. This can be a natural star or a laser producing fluorescence in the atmosphere [21]. Then such information is fed to a DM, in order to restore the image quality.

The above principle has been applied for moderate scattering samples imaged through linear fluorescence microscopy. This method consists of artificially inserting a small secondary light source (i.e. a fluorescent bead) inside the sample [22] which is fixed after its preparation. This allows for a direct measurement of the sample aberrations using a Shack-

#154177 - $15.00 USD Received 7 Sep 2011; revised 17 Oct 2011; accepted 20 Oct 2011; published 25 Oct 2011

Hartmann (SH) WFS, therefore allowing the correction of the excitation beam aberrations. However, since this technique is based on the introduction of beads inside the sample by using a microinjection needle or negative pressure protocols [22], it is prone to cause sample damage, limiting its potential for *in vivo* imaging studies. Besides, this, beads are randomly distributed inside the fixed sample, therefore a suitable bead placed at the right location should be found in the field of view (FOV) and for each depth to be imaged. This adds complexity to the sample preparation and to the aberration measurement process.

In order to extend the guide star concept for microscopy applications, a key point not properly appreciated before is that fluorescence, being an incoherent process, does not contain information about the aberrations gained by the excitation beam. Therefore, it allows for the implementation of single pass aberration measurement schemes.

Two-photon excited fluorescence (TPEF) naturally produces a small confined volume which can be used as an incoherent secondary light source. Thus in this work we show how this point source, which we refer to as the 'nonlinear guide-star' (NL-GS), can be used in a practical and noninvasive way for single pass measurements of sample and objective aberrations in NLM using a SH WFS sensor. Furthermore, we also show that this information can be used for correcting such aberrations in a single step with the help of a DM. This is demonstrated using both fixed and *in vivo* biological samples in which the enhancement of the corrected images, when compared with the non-corrected ones, results in an improvement of more than one order of magnitude in the total collected signal intensity.

2. Materials and methods

2.1. Experimental setup

The experimental setup (Fig. 1) was based on an inverted microscope (Nikon, Japan, Eclipse TE 2000U) modified to work as a laser scanning TPEF microscope. A Kerr lens mode locked Ti:sapphire laser (Coherent, Santa Clara, California, USA, Mira 900f) operated at central wavelengths of 810 and 860 nm, having a pulse duration of 100 fs and repetition rate of 80 MHz was employed to excite *in vivo* and test samples with average powers ranging from 1.5 to 5.6 mW (measured at the sample plane).

The microscope is equipped with a pair of x-y galvanometric mirrors (GM) (Cambridge technology, Lexington, Massachusetts, USA, 6215H). The NL signal was collected by a photomultiplier tube (PMT) (Hamamatsu, Japan, H9305-03), located at one of the microscope output ports. A custom made LabView interface was used to control both scanning units and the data acquisition. A filter cube, containing a short pass dichroic filter (Chroma, Bellows falls, Vermont, USA, 750dcspxr, transmittance: 440-720nm, reflectance: 800-900nm) and a BG39 band pass filter (Schott, Germany, transmittance: 320-720nm) were used to separate the excitation beam from the generated TPEF signal. A 60x oil immersion microscope objective with NA = 1.4, (Plan Apo, Nikon, Japan) was used for most of the experiments. A similar objective (CFI Apo 60x Oil λS, Nikon Japan) with enhanced transmission was used for imaging the brain slice tissue. Such objectives possess a high NA that ensures that all the available NA on the system is used, limited only by the refractive index of the sample.

A SH WFS (Imagine Optic, France, HASO3 32) was located at one of the output ports of the microscope. A lens, L5, together with the tube lens, TL, were placed to conjugate the entrance pupil of the objective into the SH WFS. This allows for the WF measurements coming from the NL-GS. As the WFS (that is based on a standard CCD camera) sensitivity is of less than a few nanojoules, the integration time needed to measure such WF can be adjusted between 0.5 s and 1 s.

To perform the aberration correction, an electromagnetic DM (Imagine Optic, France, mirao 52-e), with a ±50 μm peak to valley WF amplitude stroke, was used.

Two pairs of telescopes were used to adjust the excitation beam diameter. These were also employed to conjugate the objective pupil with the DM (L2-L4) and the with the GMs

#154177 - $15.00 USD Received 7 Sep 2011; revised 17 Oct 2011; accepted 20 Oct 2011; published 25 Oct 2011

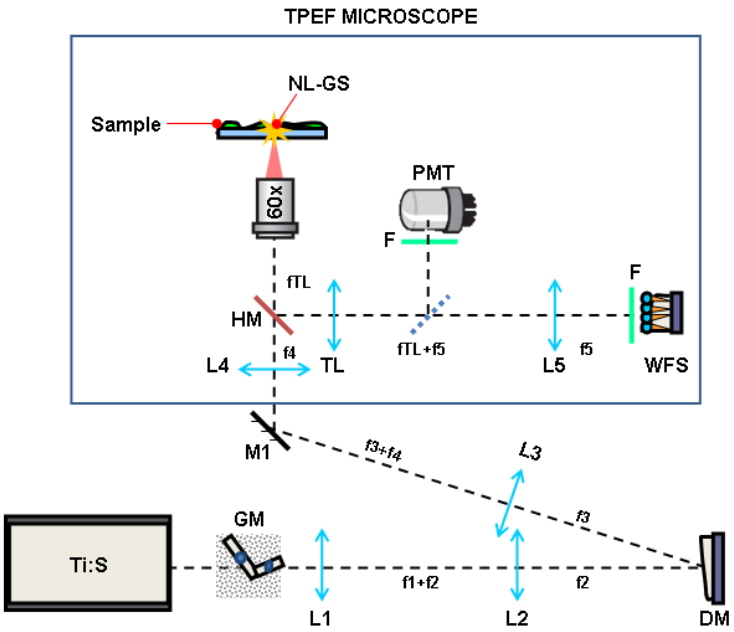

Fig. 1. Schematic experimental setup used for aberration measurements and wavefront correction. Ti:S is the Ti:sapphire laser, GM are the galvanometric mirrors, L#, lenses; DM is the deformable mirror, M#, mirror, HM is a dichroic filter, TL is the microscope tube lens, F is BG39 filter, NL-GS is the nonlinear guide-star, WFS is the wavefront sensor, and PMT is the photo multiplier tube. The microscope output port is manually selected either for the PMT or for the WF sensor. For optimum usage of the DM, it was placed as close to normal incidence as the optics mounts allow it.

(L1–L3). Both elements, the WFS and the DM were conjugated one to each other and controlled by dedicated software allowing open and closed loop control (Imagine Optic, France, Casao software).

2.2. Test-sample preparation

For the first part of this work (section 3.1), four fluorescent test-samples were used. The first two consisted of conventional red and orange water paint in water solution [23,24] applied onto a 170 µm thickness cover glass (EMS, Hatfield, Pennsylvania, USA). The dried samples had a final average thickness of ~40 µm. These were placed directly at the sample plane of the microscope. The emitted fluorescent spectrum from both test samples had a bandwidth of 40 nm (measured at the full width half maximum) centered at 550 and 600 nm, respectively.

The two remaining test-samples consisted of 1 µm and 0.28 µm diameter fluorescent microspheres (Duke Scientific Palo Alto, California USA) in water solution sandwiched between two cover glasses. The emitted fluorescent spectrum was centered at 508 nm.

2.3. Biological sample preparation

Caenorhabditis elegans samples, a widely used model organism for biological studies was employed for the *in vivo* correction trials (section 3.3). The strain was grown in nematode growth media and feed with OP50 (*Escherichia coli*).

This nematode expresses the “cameleon” (calcium indicator) [25] fluorescent protein in the pharyngeal region. Such protein is composed of four domains: cyan fluorescent protein (CFP), calmodulin, M13 (a calmodulin binding domain), and yellow fluorescent protein (YFP). For these particular set of experiments only the TPEF signal from the CFP was excited using 860 nm.

#154177 - $15.00 USD Received 7 Sep 2011; revised 17 Oct 2011; accepted 20 Oct 2011; published 25 Oct 2011

Adult worms were anesthetized using 0.8 µl of 25-mM sodium azide (NaN_3) and mounted in 3 different arrangements in order to have an additional interface, producing different magnitudes index mismatch and scattering effects. These were: i) A sample preparation where the nematodes were sandwiched between two cover-glasses, ii), a sample having a 1% agar pad of 90 µm (Scharlab, Spain AG00200500) facing the microscope objective with the nematodes mounted on top, sandwiched between two cover glasses, and iii) a sample preparation with the same mounting procedure as the second one, but having an agar pad with a final concentration of 2%. The preparations were sealed using melted paraffin and were imaged at room temperature.

With the aim to obtain mice expressing green fluorescent protein (GFP) in sparsely distributed neurons in the cortex, DNA construct CAG-GFP (1 µg/µl) was electroporated in embryonic day 15 animals by in utero electroporation as described previously [26]. After birth, animals were allowed to develop normally to collect brains at postnatal day 16. Animals were perfused and mouse brain slices having a total thickness of 60 µm (cut on a cryostat) where obtained. These were placed on a bottom glass Petri dish containing fresh medium to keep the slice in optimum conditions. The preparations were imaged at room temperature.

3. Results and discussion

3.1. NL-GS validation

The first step was to verify that a NL-GS can be used to perform WF measurements inside a sample using our SH-WFS. To do that we first parked the beam in the desired region to generate the TPEF signal (i.e. the NL-GS). This, being an incoherent process, does not retain the aberrations of the excitation beam, and therefore it can be used to measure sample induced aberrations. To do this, we arbitrarily shaped the DM to change the WF of the excitation beam while observing the TPEF of the red-paint test sample. The WFs of the excitation beam are displayed in Figs. 2(a-c) where an RMS variation of 70% (from 0.079 µm to 0.261 µm RMS) can be observed for the three different cases. As expected, this change of illumination conditions, produced similar NL-GS WFs (see Figs. 2(d-f)) having a dispersion of only a 7% on its RMS value (from 0.252 µm to 0.271µm RMS). The only difference that could be observed is a variation of the generated NL-GS brightness (the lower the aberration, the higher

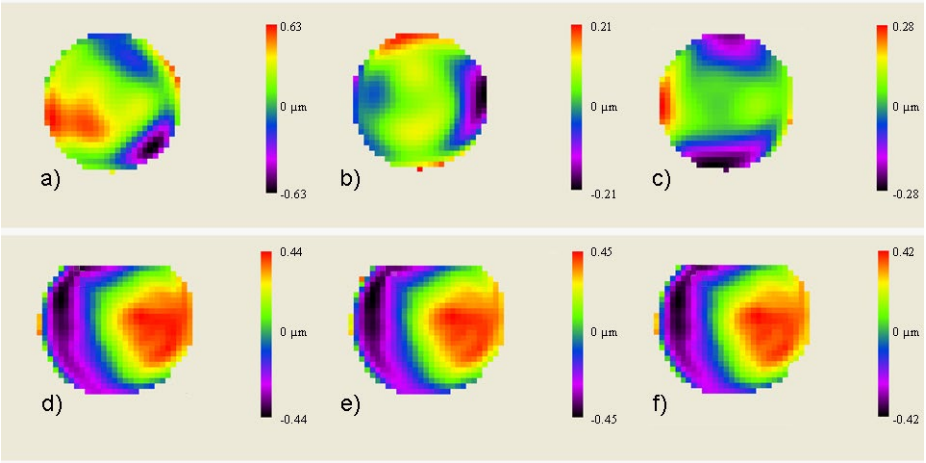

Fig. 2. (a, b, c) three different WFs of the excitation beam showing an RMS variation of up to 70% and (d, e, f) their corresponding generated WFs measured using the SH WFS. The measured NL-GS WF is similar in all three cases, with a maximum WF error variation of 7% (from 0.252µm to 0.271µm RMS). RMS: root mean square; PV: peak to valley. The planes (tilts) and spherical (focus) components of the WFs have been removed.

#154177 - $15.00 USD Received 7 Sep 2011; revised 17 Oct 2011; accepted 20 Oct 2011; published 25 Oct 2011

the collected signal). This shows that NL-GS is both, reproducible, reliable and independent from the excitation beam aberrations.

Our second step was to verify that a NL-GS behaves as point source, enabling the WF measurement inside a sample using our SH WFS. To do that we measured the WF generated by a NL-GS, i.e., from the PSF generated by the two-photon excited fluorescent volume, inside the red-paint and then we compared it with the generated WF produced by a physical point source such as a fluorescent spherical bead of i) 1 μm and ii) 0.28 μm in diameter. All three samples were placed in the same substrate in order to preserve the same experimental conditions, thus enabling us to switch between samples by only changing the cover slip lateral position. The measured WF maps are shown in Fig. 3. The resulting root mean square (RMS) WF error is similar for the three cases having an average dispersion of 8%, indicating that the WF measured by the NL-GS is not affected by the fact of having a confined focal volume created by the NL effect. Finally, the Zernike coefficient analysis in this case showed that in the three samples, the dominant aberration is coma at 90°.

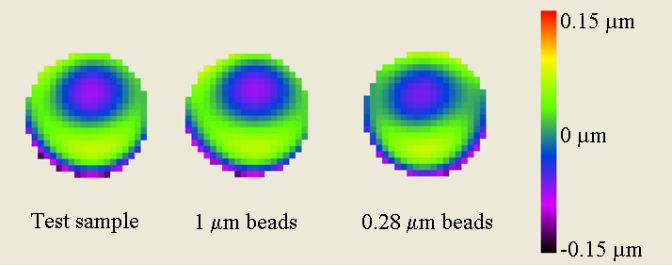

Fig. 3. Recorded wavefront maps of three different WFs generated from i) NL-GS produced inside the red-paint test-sample, ii) from 1 μm radii fluorescent beads, and iii) 0.28 μm. radii fluorescent beads. The RMS values are 0.042, 0.040, and 0.037 μm, respectively. The planes (tilts) and spherical (focus) components of the WFs have been removed.

Our third and final step is to measure the isoplanatic patch in a thin sample (to get rid of sample aberrations). This effect is described in astronomy by the isoplanatic angle which describes the maximum allowable displacement between the location of the natural guide-star and the real object to be imaged [21]. Usually aberrations are more efficiently corrected near the region where the measurement is taken in comparison with the surrounding areas. This can be verified taking advantage of the fact that the NL-GS can be placed in the exact location where the correction is required. In particular, for this experiment we recorded the WF of 9 NL-GSs, one on-axis and the remaining ones at equidistant positions of ~17.9 μm apart from the center (the complete FOV for this experiment was of ~44.8 μm). This was performed in two of our paint samples and considering two different regions on each sample in order to test the repeatability of the results. Figure 4 is an example of the WF maps recorded (results depicted for the orange-paint test-sample). All our measurement trials demonstrated that even if the immersion fluid, cover-glass and sample region, are changed, the aberrations are similar in all the FOV. This is consistent with the quality of the employed microscope. Therefore, the aberrations contained in the imaged area can be effectively acquired with only one NL-GS. For the case of an on-axis NL-GS measurement, this agrees with previous works, where a central pixel was iteratively corrected (employing a sensor-less approach) accounting for most of the aberrations present in the entire FOV [16]. Furthermore, in thicker, more inhomogeneous samples or when a larger field of view is required, multiple NL-GS can be acquired by placing them at different positions within the FOV. This would enable the correction of a wider area or volume as it will be shown in section 3.3.

#154177 - $15.00 USD Received 7 Sep 2011; revised 17 Oct 2011; accepted 20 Oct 2011; published 25 Oct 2011

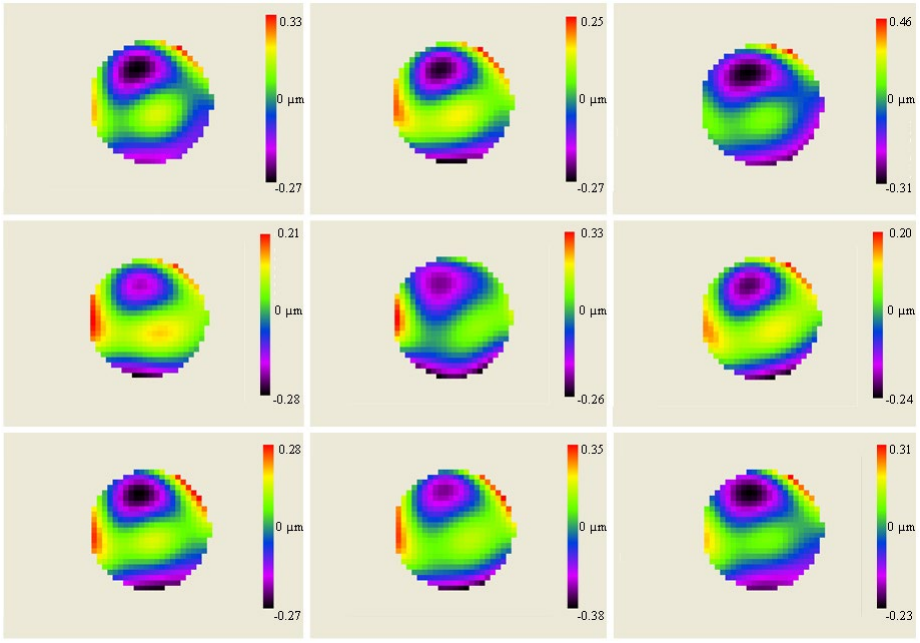

Fig. 4. Recorded off-axis NL-GS at 8 equidistant locations from the on-axis position (average RMS WFE is ~0.120 µm). The 8 recorded positions were ~17.9 µm apart from the center (RMS WFE is ~0.114 µm). The FOV for this experiment was ~44.8µm. The planes (tilts) and spherical (focus) components of the WFs have been removed.

3.2. Aberration correction strategy

To properly asses the aberrations coming from the NL-GS, it is important to first eliminate the passive aberrations of the microscope system. Taking into account this, the first correction was applied to the excitation beam to eliminate the aberrations introduced by the optical elements in the path that goes from the laser to the objective pupil (which we called "Coupling Aberrations"). In the present experiment we chose to do this in a closed loop configuration [21]. We located the SH WFS at the microscope objective pupil plane to measure the WF of the excitation beam. The aberrations were recorded and then the first 20 Zernike coefficients were transmitted to the AO control software. Note that coupling aberrations only need to be corrected once, resulting in a permanent calibration of this part of the system. Figure 5 shows this correction. Once Coupling Aberrations are corrected, the aberrations generated from the objective pupil to the output port of the microscope (i.e. including the conjugation lens) were measured and taken into account as a reference for all the subsequent WF measurements.

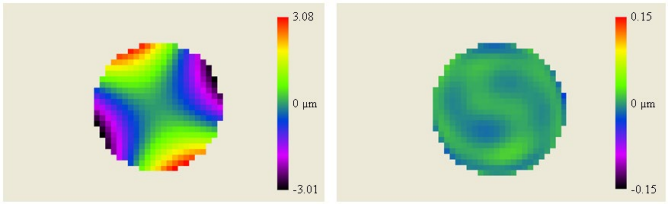

Fig. 5. Resulting system calibration correction applied to the excitation beam. Left panel excitation beam and right panel corrected beam using a closed loop configuration. The initial WFE was 1.31 µm. After the system was calibrated for coupling aberrations, the residual wavefront error was 0.007 µm. The planes (tilts) and spherical (focus) components of the WFs have been removed.

#154177 - $15.00 USD Received 7 Sep 2011; revised 17 Oct 2011; accepted 20 Oct 2011; published 25 Oct 2011

We then proceed to perform the second correction step. This consisted on measuring the aberrations caused by the focusing part of the system (called "Focusing Aberrations") which included the objective, the refractive index matching oil, the cover slip and the sample. To do that, we took into account the fact that the TPEF signal from the NL-GS is the result of an incoherent process and destroys the WF phase information of the excitation beam. Therefore the NL-GS does not inherit the coupling aberrations. Then the WF generated from the NL-GS will only contain the focusing aberrations which can be measured in a single step by employing the SH WFS. Once aberrations were measured, they were directly transmitted to the DM in a Zernike coefficients format and the DM was shaped only once. This allowed recording images in the FOV with minimized aberrations. Here it is also important to say that focusing aberrations were measured at a different wavelength from that to the excitation beam. In our methodology, we are assuming that focusing aberrations introduced in the excitation beam are similar to those introduced in the measured TPEF signal [27]. We are therefore assuming that chromatic aberration, i.e., the effect of the wavelength change, is smaller than the total contribution of our Focusing Aberrations (see section 3.3 for further discussion). Notice also that if a small amount of scattered light is produced, it would be simply added to the background without changing the recorded WFs [22].

3.3. Biological sample correction using the NL-GS

To evaluate the performance of our proposed methodology for correcting focusing aberrations, we then proceed to directly measure the WF values of the NL-GS inside a living specimen, at the center of the FOV (based on the isoplanatic patch validation) and at different depths. It is worth noticing that the produced spherical aberrations due to the oil and sample refractive index mismatch can be non-negligible and that these will not be distinguished from the aberrations produced only from the sample itself.

For the first trial we used an *in vivo C. elegans* sample sandwiched between two cover glasses. In this case corrections were performed inside the terminal bulb of the pharynx which is located between the hypodermal layers and encased in a basement membrane. As we go inside the terminal pharyngeal bulb, the structure is mainly composed of muscle. We selected the pharyngeal region of our sample as it is formed by different interfaces producing different magnitudes of index mismatch. Our experiments were performed at three different depths (corresponding to the surface, mid-plane and upper-plane of the pharyngeal region).

In Fig. 6 the three correction steps can be observed. Firstly we imaged the sample without applying any correction (Fig. 6a). Secondly we applied the coupling aberrations correction (Fig. 6b). This was followed by generating the NL-GS inside the living sample (see red spot on Figs. 6b, 6e and 6h) to correct for the focusing aberrations. Please note that the result shown in this last correction step includes both the coupling and focusing aberrations correction.

To obtain the intensity improvement in both correction steps the intensity values form all the pixels are added and then the ratio with respect to the uncorrected image is obtained. For images taken at a depth of 25μm, we measured an enhancement of 1.75 by correcting for coupling aberrations, then, the enhancement went up to 3.61 when focusing aberrations were corrected. In this case the recorded WF error was 0.16 μm and the main source of aberration was third order spherical aberration (see Figs. 6, a, b, and c). The same procedure was performed at different depths for the same pharynx (see Figs. 6 d–i). The WF errors were of 0.24 μm and 0.43 μm for images taken at a depth of 35 μm and 45 μm, respectively. In agreement with what is predicted by theoretical models [28] we found that third order spherical aberration increased approximately in a linear fashion as we collected the NL-GS deeper inside the sample (data not shown). At 35 μm an intensity improvement of 1.90 was obtained by correcting the coupling aberrations and a 2.35 by correcting the focusing aberrations. At 45 μm the improvement factor was 1.62 after correcting the coupling

#154177 - $15.00 USD Received 7 Sep 2011; revised 17 Oct 2011; accepted 20 Oct 2011; published 25 Oct 2011

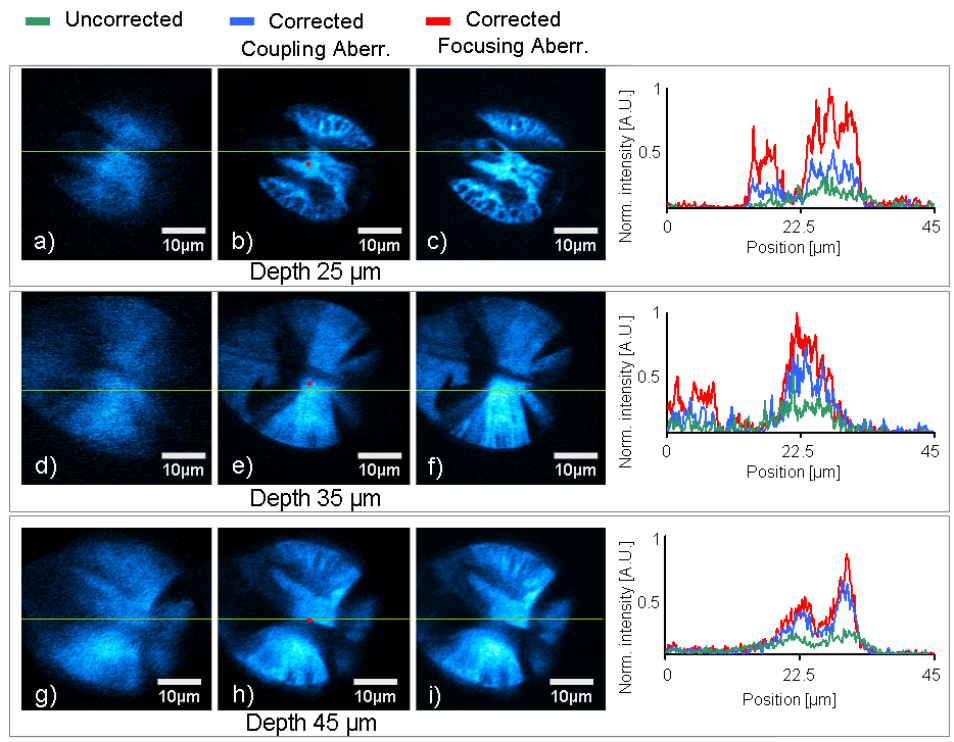

Fig. 6. Single frame images taken from an *in vivo C. elegans* sample. The imaged depths are 25 µm, 35 µm and 45 µm for the first, second and third rows respectively. The improvement factors with respect to the uncorrected case are 1.75 for (b) and 3.61 for (c); 1.90 (e) and 2.35 (f); 1.62 (h) and 2.02 (i). The gained improvement factor with respect to the coupling aberrations are 2.06 (c), 1.24 (f), and 1.24 (i). The plot profiles on the last column correspond to green line in each image. The red spot corresponds to the position where the NL-GS was measured. The WFS integration time was set to 800 ms for all the cases.

aberrations and 2.02 for correcting the focusing aberrations. As it was expected, the intensity enhancement after the correction is bounded by the amount of aberrations present in this sample [8,29,30].

In addition to the total image intensity increase after each correction step, a plot profile was traced on each image to show the normalized intensity and contrast enhancement in a specific region of interest (right column in Fig. 6). Importantly, the background signal (dark parts of the images) remains unchanged (no noise has been introduced after the correction). As a consequence, this directly gives an improvement in the contrast. As we go deeper inside the sample we expect greater intensity improvements compared to the corrections made at the superficial layers. This is, however, not the case for Fig. 6i. This could be due to experimental variables inherent of working with living samples such as sample preparation, positioning, increased scattering etc. Nonetheless, this experiment demonstrated that the NL-GS is able to capture the sample induced aberrations inside a living specimen in a noninvasive way. The use of this methodology eliminates the need of complex algorithms and the process of acquiring multiple images being able to minimize photobleaching effects. At the same time it provides the required information in a single and quick measurement to achieve an overall intensity improvement.

In what follows (see Figs. 7, 8), the nematodes are placed at larger depths in order to verify if the unexpected correction deviation observed in Fig. 6i is preserved. Furthermore for the next set of experiments we tested the NL-GS principle at increased depths by adding an additional interface and a scattering media. In this case we used a 1% agar pad as it has a

#154177 - $15.00 USD Received 7 Sep 2011; revised 17 Oct 2011; accepted 20 Oct 2011; published 25 Oct 2011

similar refractive index to deep epidermis and basal layers of skin [31]. The final thickness of such interface was 90 µm (see materials and methods). Our worm was placed on top of this layer, and the total imaging depths were 115 µm, 125 µm and 135 µm (similar depths were imaged inside the nematode than the ones acquired in the previous experiment plus the 90 µm agar pad). In this way we would work by the limit of the working distance of our high numerical aperture microscope objective. We then proceeded to perform the correction steps as explained before and at different depths inside the sample. The results are presented in Fig. 7.

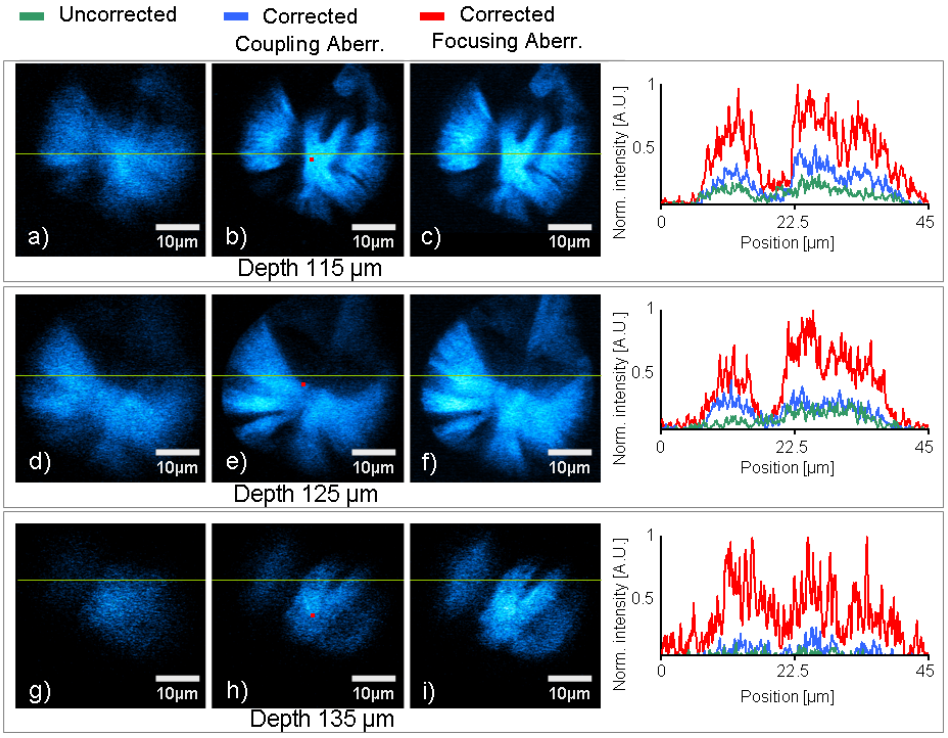

Fig. 7. Single frame images taken from an *in vivo C. elegans* sample. The imaged depths are 115 µm, 125 µm and 135 µm for the first, second and third rows respectively. The improvement factors with respect to the uncorrected case are 1.89 for (b) and 5.32 for (c); 1.58 (e) and 4.78 (f); 1.29 (h) and 9.1 (i). The gained improvement factor with respect to the coupling aberrations are 2.82 (c), 3.03 (f), and 7.08 (i). The plot profiles on the last column correspond to the green line in each image. The red spot corresponds to the position where the NL-GS was measured. The WFS integration time was set to 800 ms for all the cases.

We found that the agar pad increased the WF error by an average factor of ~4.5 times and for third order spherical aberration an average factor of ~3.9 times compared to what we recorded on the previous experiment. When correcting for the coupling aberrations we measured intensity improvements of 1.89, 1.58 and 1.29 (Figs. 7 b, e and h) for a depth of 115, 125 and 135 µm respectively. As the coupling aberrations were calibrated previously it results in a similar amount of correction as the one achieved in the case were no agar was placed before the sample. We then proceed to correct for the coupling aberrations, in this case the achieved intensity improvements were 5.32, 4.78 and 9.1 (Figs. 7 c, f and i) for a depth of 115, 125 and 135 µm respectively. As before, the NL-GS is able to capture the focusing aberrations even passing through a 90 µm interface that increases the amount of spherical aberrations. This steady increase in intensity can be also observed in the line profile traced in a region of interest to demonstrate the intensity improvement achieved employing the NL-GS (see green lines in Fig. 7). In addition the contrast improvement is clear since the aberration

#154177 - $15.00 USD Received 7 Sep 2011; revised 17 Oct 2011; accepted 20 Oct 2011; published 25 Oct 2011

correction only increases the points with a local maximum, while the local minima remains unaltered.

Furthermore, we wanted to thoroughly test the capabilities of our methodology in scattering samples. For this purpose two different samples were examined (see materials and methods). The first one consisted of a worm placed on top of a pad (same thickness as before) with a higher concentration of agar (2%). This made the agar pad more opaque and with an increased scattering (see Fig. 8). The second sample was a brain slice that is highly scattering (Fig. 9).

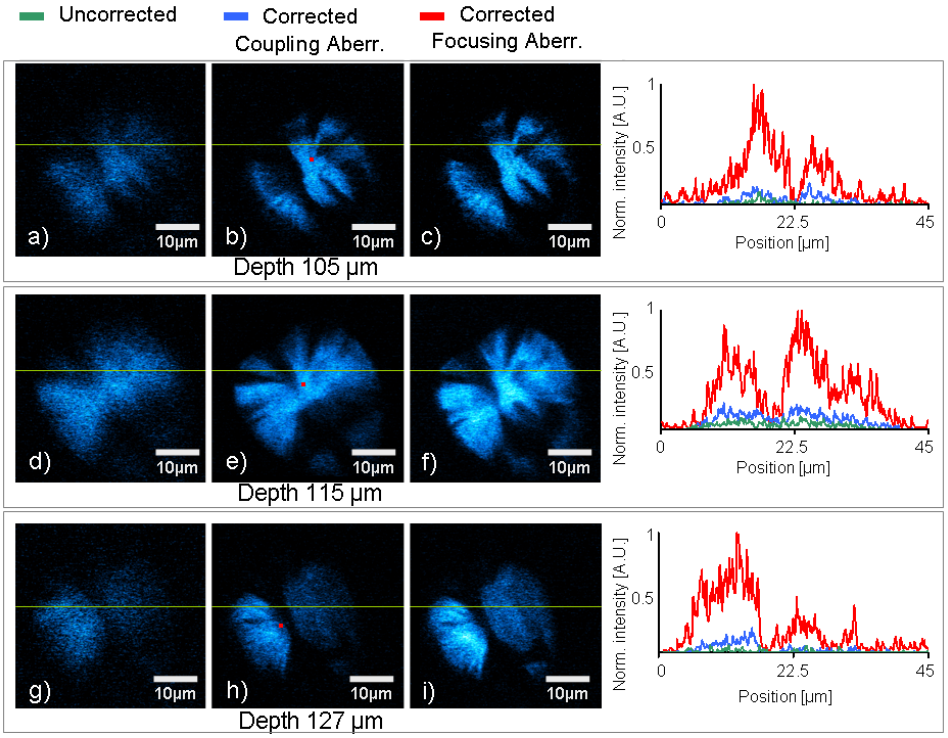

Fig. 8. Single frame images taken from an *in vivo C. elegans* sample. The imaged depths are 105 µm, 115 µm, and 127 µm for the first, second, and third rows, respectively. The improvement factors with respect to the uncorrected case are 1.70 for (b) and 17.04 for (c); 2.15 (e) and 11.24 (f); 1.94 (h) and 22.59 (i). The gained improvement factor with respect to the coupling aberrations are 10 (c), 5.23 (f), and 11.66 (i). The plot profiles on the last column correspond to the green line in each image. The red spot corresponds to the position where the NL-GS was measured. The WFS integration time was set to 800 ms for all the cases.

In Fig. 8 second column, we started by correcting the coupling aberrations having a similar correction factor as mentioned before. In this case, the RMS WF error increased by an average factor of ~5.2 times and the spherical aberration by ~4.5 times (compared with the first experiment). We achieved intensity improvements of 1.7, 2.15 and 1.94 (Figs. 8 b, e and h) for depths of 105, 115 and 127 µm, respectively. The intensity improvements after correcting for the focusing aberrations increased considerably as the amount of sample induced aberrations now play a major role limiting the intensity prior to its correction. The improvements were 17.04, 11.22 and 22.59 (Figs. 8 c, f, and i) for depths of 105, 115 and 127 µm respectively. This intensity improvement is evident as shown in the plot profile. Here the focusing aberration corrections results in a major improvement. Again, the intensity and contrast improvement caused by the aberration correction is reflected in an increase in the points having a local maximum, while the local minimum remains unaltered.

#154177 - $15.00 USD Received 7 Sep 2011; revised 17 Oct 2011; accepted 20 Oct 2011; published 25 Oct 2011

With the previous results we have shown the capability of the NL-GS methodology in situation where the main source of aberration is the sample (in this case the agar pad). In other type of specimens, the imaging depth is limited by the scattering of the tissue which changes exponentially with depth [11] (while aberration effects change linearly). Thus we proceed to apply the NL-GS concept to samples having a large scattering coefficient. In this case we selected brain slices (see materials and methods) and proceed as before, imaging two different depths. For a WF measurement in such conditions it is necessary to have at least a spot within the region of interest where the NL-GS emission is brighter (see red spot on Figs. 9b and e). Then the NL-GS is, as before, recorded by adjusting the integration time of the WFS. Figure 9 shows the obtained results.

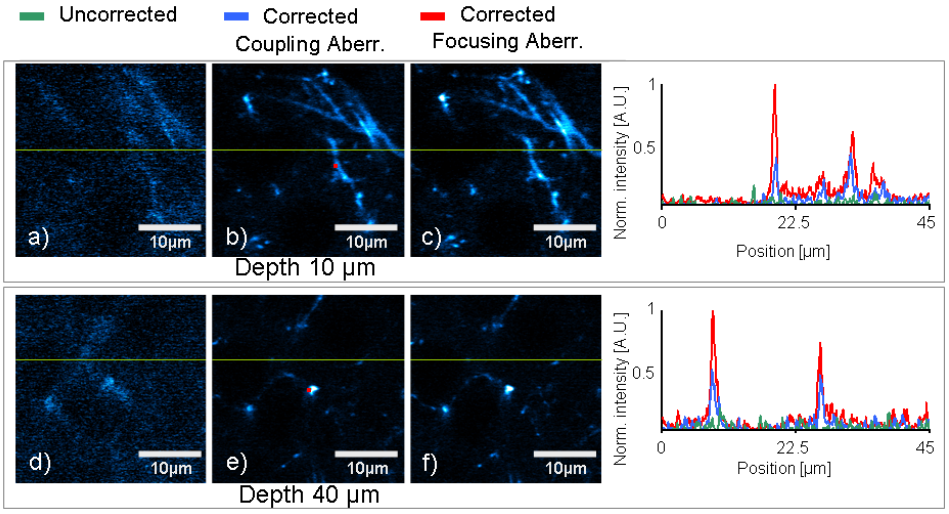

Fig. 9. Single frame images taken from mouse brain slices expressing GFP in sparsely distributed neurons. The imaged depths are 10 µm and 40 µm for the first and second rows, respectively. The improvement factors with respect to the uncorrected case are 2.74 for (b) and 5.69 for (c); 1.98 (e) and 3.91 (f). The gained improvement factor with respect to the coupling aberrations are 2.08 (c) and 1.98 (i). The plot profiles on the last column correspond to the green line in each image. The red spot corresponds to the position where the NL-GS was measured. The WFS integration time was set to 1000 ms for all the cases.

We started by correcting the coupling aberrations. Here, intensity improvements of 2.74 and 1.98 were obtained at depths of 10 µm and 40 µm, respectively (see Figs. 9 b and e). We then proceed to record the focusing aberrations. We found that these had and RMS WF error of 0.213 µm and 0.284 µm at depths of 10 and 40 µm, respectively. As before, the third order spherical aberration was dominant having a value of –0.51 µm and –0.67 µm at depths of 10 µm and 40 µm respectively. As it was expected the aberration effects remained moderate while scattering effects resulted in the requirement of an efficient excitation strategy image the sample. For that we used an IR optimized microscope objective (see material and methods). After correcting for the focusing aberrations, the resulting intensity improvements on the generated images were 5.69 and 3.91, at 10 µm and 40 µm respectively.

By comparing the results obtained for both, moderate (Figs. 6–8) and strongly scattering samples (Fig. 9), we observe that AO has a larger impact on the correction for moderate scattering specimens, as they allow imaging at deeper planes. For more scattering samples, we have found that a correction is still possible and our measured improvements are in agreement with those achieved by using other sensor-based adaptive optics correction schemes (~2) [11]. However, scattering will dominate as the imaging goes deeper. This suggests the requirement of more power to image the sample or the use of other strategies such as the use of index matching media inside *in vitro* samples to reduce scattering [16].

#154177 - $15.00 USD Received 7 Sep 2011; revised 17 Oct 2011; accepted 20 Oct 2011; published 25 Oct 2011

At this point, it is important to remember that for this particular experiment, the NL-GS was created at different depths (i.e. at the plane where the correction was required). In addition, based on our isoplanatic patch measurements we placed the NL-GS only at the on-axis position. Nevertheless, to verify these results, a line profile was traced (see the green line of Figs. 6, 7, 8, 9) at different locations from the on-axis position. Also in this case, the improvement obtained after the correction is still significant. This means that field aberrations are not a limiting parameter within the considered samples and microscope objectives. In addition, by using the NL-GS concept one can take advantage of the fact that the position of this reference light source is always kept on hands of the user and several FOV corrections, using different NL-GS, could be considered for a particular study. Then, as it is done in multi laser guide-star telescopes, stitching methods should be considered for the reconstruction of the final aberration corrected images. Similarly, as it was shown, several NL-GS can be collected for different depths in thicker samples. This means that in general, such principle could be used, according to the requirements of each sample, for acquiring aberration-corrected 3D images.

Note that the correction of the excitation beam is based on a measurement that has been done at a different wavelength (fluorescence signal). This shift however did not affect our method, resulting in a clear signal intensity and contrast improvement as it can be seen from Figs. 6, 7, 8 and 9. This independence of the correction with the wavelength shift is probably due to the employed microscope objectives, which are corrected for chromatic aberrations from UV to IR. Our results agree with previous works where chromatic effects have already been reported to be negligible over a significant wavelength difference [27,32].

Finally, in many applications, the numerical aperture of the imaging system could be limited by the refractive index mismatch of the sample (for example when imaging microfluidic channels), introducing significant aberrations. The technique here presented can be used to overcome this situation and to obtain a resolution closer than that given by the system.

4. Conclusions

We have introduced the NL-GS concept to correct the measured aberrations induced by the sample and the objective in a single-step. This NL-GS is created by focusing the excitation beam inside the sample to produce a TPEF spot which is considered as a secondary light source. Furthermore, based on the fact that fluorescence is an incoherent process, it does not inherit the aberrations gained by the excitation beam.

The WF from the NL-GS can then be measured using a WFS placed at the output port of the NLM microscope. Moreover, as the WF is directly expressed in the form of Zernike coefficients, it is possible to shape the adaptive element (DM) in a single step (i.e. without the need of any search algorithm) for correcting the measured aberrations. By doing so, image quality and contrast can be significantly improved without having to expose the sample for large periods of time. Consequently photo-bleaching and photo-toxicity are greatly reduced.

The proposed methodology brings several advantages: it can be applied *in vivo*, it is simple, noninvasive and requires no additional sample processing (such as the incorporation of fluorescent beads). Moreover, the NL-GS can be created at any desired position inside a sample. This principle has been demonstrated with both, moderate and increased scattering samples. For moderate scattering samples, when comparing coupling vs. focusing aberrations, we found that the total signal improvement can be up to 11.66 times (see Fig. 8i). For samples with increased scattering, we have found that the correction is moderate but in agreement with other adaptive optics correction schemes [11]. All this demonstrates that, under the high resolution conditions (NA = 1.4) here used, this methodology is able to successfully deal with the aberrations present in the imaging system. Overall, this technique can be successfully employed in a great number of cases, for example in microfluidic channels or in general for

#154177 - $15.00 USD Received 7 Sep 2011; revised 17 Oct 2011; accepted 20 Oct 2011; published 25 Oct 2011

other biological applications where a high resolution (i.e., not limited by the refractive index of the sample) is required.

Acknowledgments

This work is supported by the Generalitat de Catalunya grant 2009-SGR-159, the Spanish government grants TEC2009-09698 and SAF2008-00211, the EU project STELUM (FP7-PEOPLE-2007-3-1-IAPP, 217997) and the NoE P4L and Laserlab optobio. We thank Dr W. Schafer from the MRC Laboratory of Molecular Biology (Cambridge, UK) for providing the *C. elegans* strain, and Nikon instruments Spain for providing the microscope objectives used in this work. This research has been partially supported by Fundació Cellex Barcelona and has been conducted at ICFO's "Super-Resolution Light Microscopy and Nanoscopy Facility" (SLN@ICFO).

#154177 - $15.00 USD Received 7 Sep 2011; revised 17 Oct 2011; accepted 20 Oct 2011; published 25 Oct 2011